

# Journal of Materials Chemistry B

Accepted Manuscript



This is an *Accepted Manuscript*, which has been through the Royal Society of Chemistry peer review process and has been accepted for publication.

*Accepted Manuscripts* are published online shortly after acceptance, before technical editing, formatting and proof reading. Using this free service, authors can make their results available to the community, in citable form, before we publish the edited article. We will replace this *Accepted Manuscript* with the edited and formatted *Advance Article* as soon as it is available.

You can find more information about *Accepted Manuscripts* in the [Information for Authors](#).

Please note that technical editing may introduce minor changes to the text and/or graphics, which may alter content. The journal's standard [Terms & Conditions](#) and the [Ethical guidelines](#) still apply. In no event shall the Royal Society of Chemistry be held responsible for any errors or omissions in this *Accepted Manuscript* or any consequences arising from the use of any information it contains.

# Versatile Fabrication and Applications of Dense, Orderly Arrays of Polymeric Nanostructures over Large Areas

Chang Quan Lai<sup>1,\*</sup>, H. Cheng<sup>1</sup>

<sup>1</sup>Advanced Materials for Micro- and Nano-Systems Programme, Singapore-MIT Alliance,  
National University of Singapore, Singapore 117576, Singapore

Email: laicq@mit.edu

## Abstract

Dense arrays of nanostructures were fabricated in polymer surfaces over large areas (1 cm x 1 cm) using laser interference lithography and low power CF<sub>4</sub>/O<sub>2</sub> plasma etching. The dependence of etch rate and etch anisotropy on plasma composition was studied in detail for polystyrene and 4 distinct regimes were identified. In each of these regimes, the polystyrene nanostructures exhibit characteristic variations of etch rate, etch anisotropy and surface chemistry that were found to be closely related to the level of fluorination and polymerization on the substrate surface. A new technique, stitch etching, was developed and utilized in conjunction with low power plasma etching to increase the height of nanostructures without loss of array density. These nanofabrication techniques are shown to be versatile enough to be applied to a variety of polymers. The polymeric nanostructures were found to exhibit a number of useful properties including superhydrophobicity (directional effect, lotus leaf effect and rose petal effect), structural stiffness and biocompatibility, which were shown to be useful in applications such as self-cleaning surfaces, nanoimprinting molds and biocompatible substrates for neurite guidance.

## Introduction

Polymeric nanostructures have raised great research interest in photonics<sup>1,2</sup>, micro-/nano-fluidics<sup>3</sup> and biology<sup>4,5</sup> due to their unique combinations of thermal, electrical, mechanical, optical and biocompatible properties with low cost and ease of processing. Currently, the most popular method of fabricating polymeric nanostructures is nanoimprinting, which offers the advantages of simplicity, large area processing and unperturbed chemistry of the polymer. However, this technique suffers from drawbacks such as high cost of molds, limited life of release coatings, inflexibility (a single mold cannot produce different sidewall profiles or switch between global and local pattern transfer) and possible loss of pattern fidelity due to thermal expansion coefficient mismatch between the mold and polymer.<sup>6</sup> In contrast, low power plasma etching, combined with a flexible maskless patterning technique such as laser interference lithography, avoids such issues and offers an alternative method for fabricating large areas of polymeric nanostructures in a cost-effective manner. This approach also has the advantage of combining nanostructure formation and chemical functionalization of the nanostructure surfaces in a single step.

Although the use of plasmas in polymer etching is not new, previous efforts have mostly relied only on the physical bombardment of ions at high rf power/external bias (i.e. reactive ion etching) to obtain nanostructures with anisotropic sidewalls.<sup>7,8</sup> This method generates a significant amount of heat as compared to low power plasma etching and thus, is incompatible with the majority of commercial polymers which possess relatively low softening temperatures or melting points.

In this study, we investigated how the  $\text{CF}_4/\text{O}_2$  plasma composition can be manipulated to impart anisotropy to low power plasma etching so as to produce dense arrays of high aspect ratio nanostructures in polystyrene surfaces. We also show that imperfect anisotropy of plasma etching can be exploited to further improve the height of nanostructures through a

new patterning technique we refer to as stitch etching. The versatility of this fabrication method was then investigated with a variety of polymers including Kapton polyimide, polypropylene and polyethylene terephthalate (PET). Finally, the properties of polystyrene nanostructures fabricated with low power plasma etching were characterized and evaluated for various applications.

## Experimental Procedure

### Fabrication of Nanostructures

Commercial Polystyrene (PS) compact disc protective case covers, Polypropylene (PP) file covers, 3M Kapton® Polyimide tape #5413 (PI) and Polyethylene Terephthalate (PET) transparencies were used in this study to fabricate nanogratings, nanopillars and nanofins. The surface roughness of these polymers was characterized using a surface profiler, Alpha Step 500, from Tencor Instruments and was found to be approximately 10 nm-30 nm while long distance (over 500  $\mu\text{m}$ ) undulations can have amplitudes up to 75 nm.

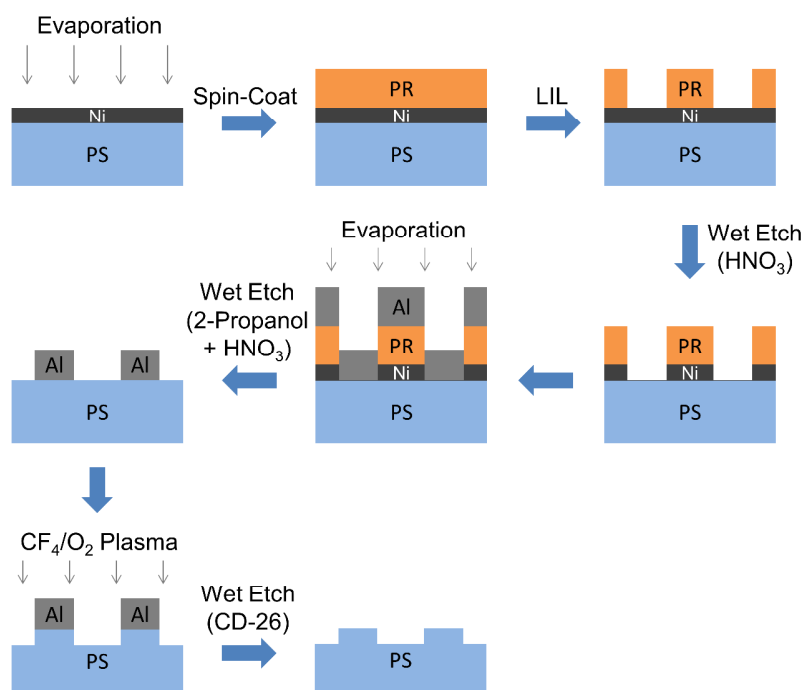


Figure 1: Schematic diagrams describing the process flow for the fabrication of polymeric nanostructures using low power  $\text{CF}_4/\text{O}_2$  plasma etching. PR – Photoresist. PS – Polystyrene. LIL – Laser interference lithography.

The polymers were cleaned with 2-Propanol and rinsed with de-ionized (DI) water. Figure 1 summarizes the process flow for the fabrication of the polymeric nanostructures. A 7 nm layer of 99.9% pure Ni was thermally evaporated onto the PS substrate to act as an adhesion layer for photoresist. After dicing the PS substrates into 1 cm x 1 cm samples, 1  $\mu\text{m}$  of photoresist (Ultra-i-123) was spin coated onto each sample and laser interference lithography (LIL) was performed with the Llyod's mirror setup<sup>9</sup> using a He-Cd laser (wavelength = 325 nm). Nanogratings were patterned with a single exposure while nanopillars were patterned with two exposures at right angles to each other. Nanofins were also patterned with a double exposure, with the second exposure at an in-plane angle between 0° and 90° with respect to the first exposure. Nanostructures were fabricated with a consistent period of 630 nm across the entire patterned area for all samples in this study, unless stated otherwise. For nanostructures to be patterned on specific areas on the substrate, an additional exposure of the photoresist using conventional photolithography and an optical mask can be carried out. After development of the photoresist with a commercial etchant, Microposit MF CD-26, which consists mostly of dilute tetramethylammonium hydroxide, selective wet etching of the Ni layer was performed using concentrated  $\text{HNO}_3$  (60wt%). A layer of 99.9% pure Al (40 nm) was then thermally evaporated onto the samples and selective wet etching of the photoresist and remaining Ni leaves behind an Al layer with an inverse pattern on the PS substrate.

Plasma etching of polymer samples was performed at room temperature with an rf power of 40 W (at 13.56 MHz), a chamber pressure of 0.04 Torr and a total flow rate of  $\text{CF}_4$

and O<sub>2</sub> fixed at 10 sccm. The sample was placed at the anode which is grounded and has a diameter of 28 cm (cathode diameter is 22 cm) and no external dc bias was applied. After plasma etching, Al and any deposited polymers were removed from the samples with Microposit MF CD-26.

### **Etch Rate Measurements**

To measure etch rates, half of each plain PS sample (1 cm x 1 cm) was covered with 3M Kapton® Polyimide tape (#5413) and subjected to the desired etching process for 5-10 minutes. After that, the tape was removed and 5 readings from each sample were taken with an Alpha Step 500 (Tencor Instruments) to determine the height difference between the covered and exposed regions of the substrate. The samples were then immersed in the Microposit MF CD-26 for 5 minutes to remove any plasma deposited polymer layers. After drying with a nitrogen air-gun, another 5 readings were taken. The difference between the first and second set of readings will then give the thickness of the deposited polymer, if any. A paired, two-tailed student's t-test was also carried out to ensure that the difference between the 2 sets of readings was statistically significant ( $p < 0.01$ ).

### **Imaging**

For the scanning electron micrograph (SEM) experiments, a layer of 20-40 nm of Al was thermally evaporated onto the samples to reduce charging effects. SEM pictures were taken with an FEI NOVA NanoSEM 230 or Philips XL30 at an accelerating voltage of 3-5kV.

### **X-ray induced Photoelectron Spectroscopy**

The X-ray induced Photoelectron Spectroscopy (XPS) (Mono Al K $\alpha$  radiation at 1486.71 eV) experiments were carried out to determine the proportion of C, O and F in the

PS surface after  $\text{CF}_4/\text{O}_2$  plasma treatment. The quantities of O and F were separately expressed as a percentage of the total amount of C, O and F present on the surface. XPS was also used to probe the composition of polymers deposited during the course of plasma etching. Results were processed and analyzed using the XPS Peak program (version 4.1).

### **Water Contact Angle Measurements**

The water contact angle measurements were performed at room temperature with VCA Optima XE (AST Products Inc) using the sessile drop method. Five independent sets of readings were obtained for each sample.

### **Nanoimprinting**

PDMS nanostructures were fabricated by pouring a mixture of PDMS base and curing agent (Sylgard 184 Silicone Elastomer Kit from Dow Corning) in 10 to 1 ratio into PS molds which had been coated with anti-sticking agent ([tridecafluoro-1,1,2,2-tetrahydrooctyl] trichlorosilane from Gelest Inc.). The mixture and mold were cured at  $70^\circ\text{C}$  for 3 hours.

### **Cell Culture**

PS nanostructures (width = height = 500 nm) were sterilized with UV for 30 minutes and then immersed in 70% ethanol for five minutes to minimize contamination. PDMS was used to secure the samples to the bottom of 12-well culture plates (1 sample/well) after which each sample was immersed in 2 ml of DMEM at  $37^\circ\text{C}$  for two days in order for residual chemicals and uncured PDMS to leach out. Following that, 1 ml of Poly-D-Lysin (PDL) solution ( $0.5 \mu\text{g/ml}$ ) was deposited in each well for a day to enhance cell attachment to the sample surfaces.

The rat pheochromocytoma cell line PC12 (# CRL-1721; American Type Culture Collection) cells were seeded on PDL coated PS nanostructures at a density of  $3.4 \times 10^4$  cells per well. Cells were cultured with DMEM medium enriched with 10% heat inactivated fetal bovine serum (FBS) and 5% horse Serum in a incubator at 37 °C with 5% CO<sub>2</sub>. Cells were allowed to grow for two days before differentiation.

Culture medium was changed to serum depleted DMEM 24 hours prior to stimulation. PC12 cells were treated with Nerve Growth Factor (NGF) at a concentration of 50 ng/ml. Images were taken with an optical microscope before treatment and at 48 hours after treatment.

## Results and Discussion

### CF<sub>4</sub>/O<sub>2</sub> Plasma Etching

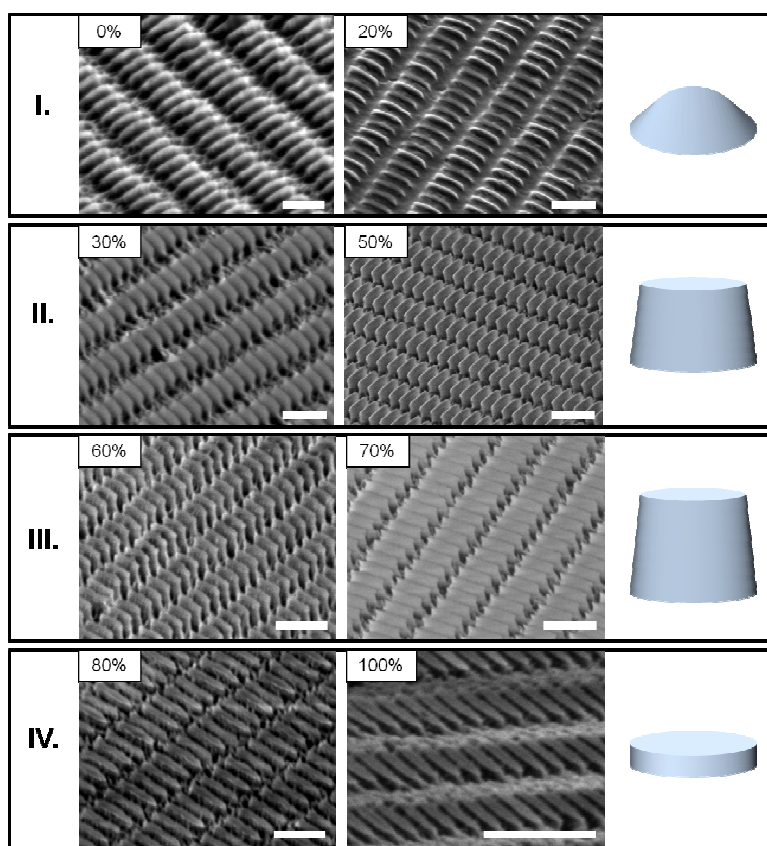


Figure 2: SEM pictures of nanofins obtained when the amount of  $\text{CF}_4$  indicated in the top left corner is present in the plasma. The nanofins are categorized into 4 types (I-IV) and schematic diagrams illustrating the characteristic morphologies for each type are shown on the right of each row. Note that charging effects in the SEM caused the nanofins fabricated with 100%  $\text{CF}_4$  plasma to seem slightly slanted. Scale bar represents 2  $\mu\text{m}$ .

PS nanofins were fabricated with varying  $\text{CF}_4$  amounts in the  $\text{O}_2$  plasma using low power plasma etching. The time of treatment for each plasma composition was adjusted with respect to its etch rate such that a constant nanostructure height of 1  $\mu\text{m}$  was expected across all samples.

SEM images of these nanofins are shown in Figure 2 and four distinct types of structures can be observed. Type I structures (Figure 2, Row I), fall short of the expected 1  $\mu\text{m}$  height and have sharp, narrow tips (tip width for 100%  $\text{O}_2 \leq 30 \text{ nm}$ ) with a rounder profile of the edges than nanofins in other regimes, which appear more rectangular. This suggests that Type I nanofins were etched with strong isotropy to the point of tip extinction before the designated height was reached (See Supporting Information I). Type II structures (Figure 2, Row II) exhibit an improved aspect ratio (up to 9 when etched to tip extinction) derived from better etch anisotropy. The highest aspect ratio (up to 12), however, was achieved for Type III structures (Figure 2, Row III) which are similar in form to Type II structures. Type IV nanofins (Figure 2, Row IV) also failed to attain the designed height but unlike Type I structures, Type IV nanofins possess broad, flat tips which indicate that etching was severely retarded and might have stopped mid-way during the plasma treatment.

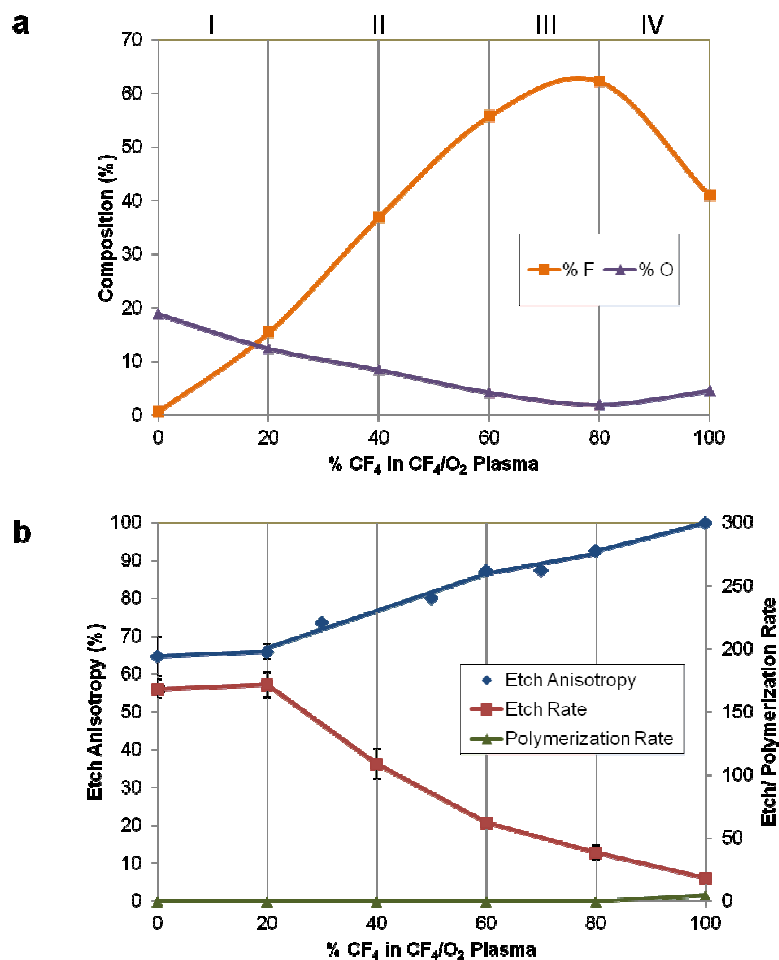


Figure 3: (a) Percentages of fluorine and oxygen found on the PS surface after plasma treatment. (b) Etch anisotropy, etch rate and polymerization rate with respect to plasma composition. The best fit line for etch anisotropy data points within each regime is also included. The range of plasma compositions that corresponds to the different types of nanofins in Figure 2 (regimes I – IV) have been color coded. Error bars indicate the standard deviation in measured values.

To understand the mechanisms that led to the formation of the four types of nanostructures shown in Figure 2, we first look at the effect of plasma composition on the surface chemistry of PS and how that affects the etch anisotropy. Figure 3a shows the

percentages of fluorine and oxygen found on the PS surface as determined using XPS measurements after plasma treatments. It can be seen that as the plasma composition shifts towards a CF<sub>4</sub> rich mixture, increasing amounts of fluorine become incorporated into the PS surface until the proportion of CF<sub>4</sub> increases beyond 80%, at which point the trend reverses and the fluorine content in the PS surface starts to dip. This variation of fluorine on the PS surface with respect to the plasma composition is very similar to that of atomic fluorine in the plasma<sup>10</sup> and it is likely that the amount of fluorine incorporated into the PS surface is directly dependent on the amount of atomic fluorine in the plasma. This is consistent with the findings of Strobel *et al.*<sup>11</sup> and Occhiello *et al.*<sup>12</sup>

Therefore, it is reasonable to see that increasing levels of fluorine were found on the PS surface from 0% to 80% CF<sub>4</sub> because the increasing proportion of CF<sub>4</sub> gas provided more and more precursors for atomic fluorine to be generated in the plasma and also shifts the electron energy distribution to higher energies, encouraging the dissociation of CF<sub>4</sub> into atomic fluorine.<sup>10</sup> This, in turn, causes more fluorine to be included in the surface with richer CF<sub>4</sub> plasma compositions. The dip in fluorine content of the PS surface for plasma compositions with ≥80% CF<sub>4</sub> is due to the decreasing proportion of O<sub>2</sub> in the plasma which, in small amounts (0% - 20%), encourages the extraction of atomic fluorine through the formation of intermediates such as COF<sub>2</sub> and OF radicals.<sup>10</sup>

At higher O<sub>2</sub> levels (>20%), however, oxygen atoms contend with fluorine atoms for radical sites on the substrate,<sup>13</sup> contributing to the fall of fluorine content in the PS surface with increasing O<sub>2</sub> content (i.e. decreasing CF<sub>4</sub> content) in the plasma. Note that the processes described above have the same but opposite effect on oxygen incorporation into PS, which explains the opposing trends of %O and %F shown in Figure 3a.

The amount of fluorine incorporated into the PS surface has important implications for the etch anisotropy and etch rates as fluorinated polymers are known to be resistant to

etching in the absence of ion bombardment.<sup>13</sup> This means that as higher levels of fluorine are incorporated into the surface chemistry, the nanostructures receive more and more protection from isotropic chemical etching, depending largely on highly directional ion bombardment for material removal to form the nanostructures. As such, the etch rate should decrease and etch anisotropy improve with increasing fluorination of the nanostructure surface. This is consistent with our observations that the etch rate falls and etching anisotropy increases from regime I (low fluorine content at the substrate surface) to regime III (high fluorine content at the substrate surface) (see Figure 3b).

Within regime I itself, however, etch anisotropy does not improve significantly even though fluorination increases from approximately 0% to 15%. Etch rate measurements exhibit the same trend as they remain largely unchanged within regime I, suggesting that a minimum level of fluorination has to be achieved before substantial alteration of the PS surface properties and subsequently, the etching mechanism, can take place.

This appears to be the case in regime II, for which, having surpassed this threshold level of fluorination, the rapid increase in surface fluorination with rising  $\text{CF}_4$  content in the plasma leads to an increasingly resilient PS surface that depends more and more on anisotropic ion bombardment to facilitate etching. As a result, the etch rate declines sharply while the etch anisotropy rises appreciably in regime II.

In regime III, the rate of surface fluorination falls considerably with increasing  $\text{CF}_4$  content as the level of fluorination approaches a maximum. Consequently, the etch rate decreases at a slower pace than in regime II and the increase in etch anisotropy is relatively modest.

In regime IV, fluorination of the PS was observed to be reduced compared to regime III. However, etch anisotropy continues to improve while the etch rate continues to fall in this regime. The cause of this was traced to the deposition of a fluorocarbon polymer in regime

IV (Figure 3b). This fluorocarbon layer, with a C to O to F ratio of 3.8: 1: 11.6, was found to be very resistant to etching. As a result, the etch rate decreases and the etch anisotropy improves as the fluorocarbon layer provides sidewall protection for the nanostructures, in much the same way as fluorinated PS protects the sidewalls against isotropic etching as described above.

Therefore, it is clear that aspect ratios of nanostructures improve from Type I to Type III due to the increasing fluorination of the substrate surface which reduces isotropic etching. This results in Type III nanostructures having both tall and steep sidewalls. Although the etch anisotropy continues to increase in regime IV due to the introduction of a etch-resistant fluorocarbon layer on the PS surface, this fluorocarbon layer also significantly retards etching, causing a limited depth of etching. For instance, we have not been able to obtain nanostructures beyond a height of 150 nm when using a 100% CF<sub>4</sub> plasma, regardless of the etching duration. Therefore, although etch anisotropy is high in regime IV, the nanostructures produced have low aspect ratios as seen in Figure 2.

It is worthwhile to note here that the aspect ratios of nanostructures formed with our low power plasma etching are better than those exhibited by polymeric nanostructures fabricated with high power plasma etching (up to  $\approx 4$ )<sup>7</sup> and comparable to those obtained using nanoimprinting (up to  $\approx 25$ )<sup>4,14-16</sup>. Although polymeric nanostructures of aspect ratios up to 60 have been made using high power plasma etching<sup>8</sup>, it should be noted that such nanopillars are not structurally uniform and the specialized process does not appear to be compatible with orderly patterns.

### **Stitch Etching**

Up to this point, the maximum height that the nanostructures can reach has been dictated by the etch anisotropy and initial mask size. To achieve greater heights, the etch

mask pads can be made larger but this method will quickly compromise the density of the nanostructures when the pad size exceeds the original period of the pattern. In order to push the nanostructure height beyond these limits without sacrificing density, the concept of stitch etching is introduced. By strategically arranging etch sites in such a way that they would join up to give the desired form of nanostructure as a result of isotropic etching (hence, the name stitch etching), the maximum height can be substantially increased for a given density of nanostructures (see Figure 4). This method is applicable only when the etch anisotropy is less than 100% as lateral etching is required for the stitching of the etch sites to take place.

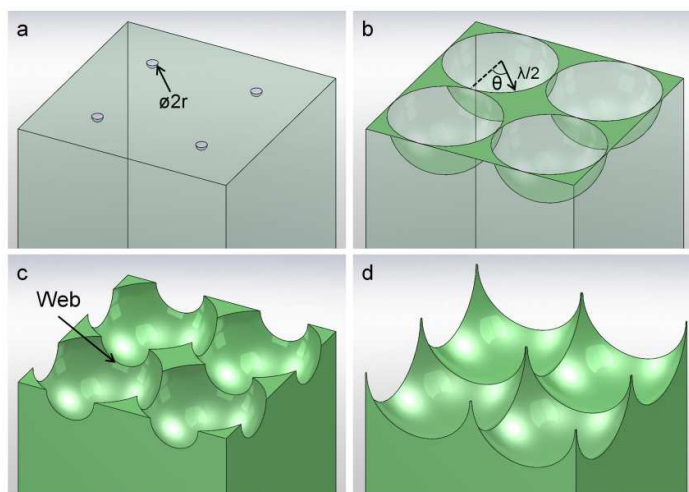


Figure 4: Stitch etching demonstrated with a rectangular arrangement of circular holes and isotropic etching. (a) Etch depth  $\approx 0$  (b) Etch depth =  $0.5\lambda$  (c) Etch depth =  $0.55\lambda$  (d) Etch depth =  $0.7\lambda$ .  $\lambda$  refers to the period of the holes. The transparency of the model is varied for clarity.

One distinct characteristic of stitch etched samples would be the interconnection of nanostructures by “webs” (Figure 4c). Such features may not necessarily be undesirable as they offer the benefits of increased surface area and provide mechanical stability for the high

aspect ratio nanostructures. The height and shape of these webs can be easily derived from the equation for etch anisotropy ( $A = 1 - D_L/H_{web}$ ) to be

$$H_{web} = \frac{D_L}{1-A} = \frac{\frac{\lambda}{2\cos\theta} - r}{1-A} \quad (1)$$

where  $H_{web}$  is the total height of the web at a given  $\theta$ ,  $D_L$  is the total lateral etch distance,  $\lambda$  is the period,  $r$  is the radius of the hole,  $A$  is the anisotropy of etching and  $-45^\circ \leq \theta \leq 45^\circ$  for rectangular arrays and  $-30^\circ \leq \theta \leq 30^\circ$  for hexagonal arrays. Note that the nanopillars that result from stitch etching are located at the maximum and minimum  $\theta$ , which, when substituted into equation (1), gives the height of these nanostructures,  $H$ .

Comparing the maximum possible nanostructure height achievable by conventional etching with a hard mask pad of radius  $\lambda/2$  and stitch etching which starts with a hole of infinitesimally small radius, it can be seen that  $\frac{H}{H_{conventional}} = \frac{1}{\cos\theta}$  where  $H_{conventional} = \lambda/2(1-A)$  and  $H = \lambda/[2\cos\theta(1-A)]$ . If a hard mask pad in conventional etching is changed into a hole of the same dimension for stitch etching instead, the improvement is given by

$$\frac{H}{H_{conventional}} = \frac{\lambda}{2r\cos\theta} - 1.$$

Applying this technique to PS nanostructures, we have achieved aspect ratios of up to 20 (see Figures 5a and 5b) and exotic structures such as ribbed nanogratings (Figure 5c) and zig-zag rows of nanopillars (Figure 5d) that cannot be easily fabricated using other methods. Although stitch etching has been applied to PS nanostructures here, it is compatible with other etching techniques (with some degree of etch isotropy) for different kinds of materials and is expected to be useful in applications that benefit from increased surface areas, such as nanocapacitors<sup>17</sup> and superwicking surfaces<sup>18-21</sup>.

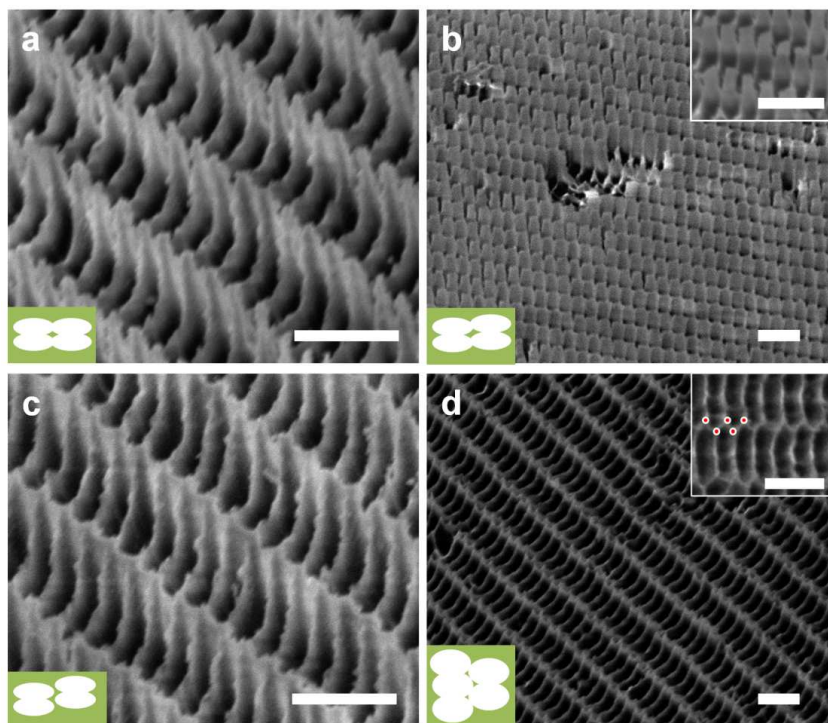


Figure 5: High aspect ratio nanostructures obtained by stitch etching. (a) Nanopillars (b) Nanofins (inset: magnified view) (c) Ribbed nanogratings and (d) Zig-zag rows of nanopillars (inset: top view. The positions of some nanopillars are highlighted in red to reveal the zig-zag arrangement). Schematic diagrams showing the formation of the structures from fin holes are shown on the bottom left. Scale bars represent 2  $\mu\text{m}$ .

### Versatility

Low power plasma etching and stitch etching can be applied to more than just PS material and nanofin patterns, as shown in Figure 6. We have demonstrated that our process can be used to nanostructure the surfaces of thermoplastic (PP, PS) and thermosetting polymers (PI, PET) with unsaturated (PS, PI, PET) and saturated moieties (PP). In addition, it was found that the nanostructures fabricated have good uniformity across the entire processed area (1 cm x 1 cm). This shows that nanostructures can be fabricated with our

method on a wide variety of polymers from commercial products with different properties that can be selected for a diverse range of applications.

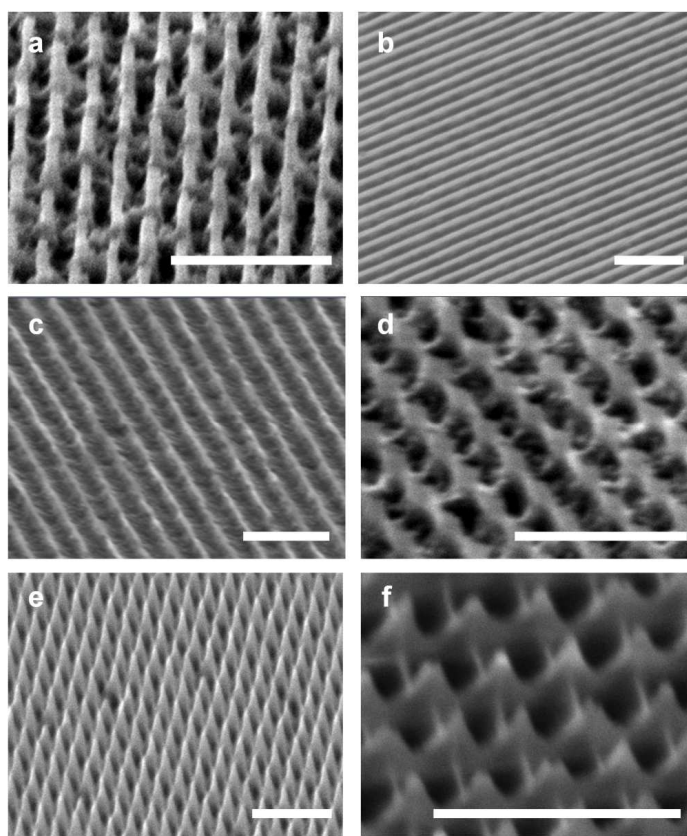


Figure 6: SEM pictures of (a) nanopillars on PS (b) nanogratings on PS (c) nanogratings on PP (d) nanopillars on PP (e) nanopillars on Kapton® PI and (f) stitch etched nanopillars on PET formed from a rectangular array of holes. Low power plasma etching was carried out with gas comprising 70%  $\text{CF}_4$  and 30%  $\text{O}_2$ . Etch anisotropy for nanopillar and nanograting patterns on PS are similar to that of nanofin patterns. Scale bars represent 2  $\mu\text{m}$ .

It is also worth noting that some of these commercial polymers are thermosets (e.g. PI) that cannot be processed by nanoimprinting as they will decompose rather than soften upon heating. To overcome this issue, nanoimprinting of these polymers will have to be carried out with the liquid precursors, instead of cost effective plastic products that are readily available

off the shelf. Once these polymers have set, nanoimprinting cannot be used for further processing but plasma etching can. Therefore, low power plasma etching can be used as an alternative to nanoimprinting.

### **Superhydrophobicity**

One of the greatest advantages of fabricating nanostructures on polymers using low power plasma etching is that chemical functionalization of the surface and nanostructure formation can be achieved in a single step, thus reducing the cost and complexity of engineering functional surfaces. To demonstrate this, we used 70% CF<sub>4</sub> - 30% O<sub>2</sub> low power plasma etching process to incorporate fluorine, which lowers the surface energy of polymers,<sup>22</sup> into the surfaces of PS nanostructures (See Supporting Information II). The feasibility of using the resulting PS nanostructures as superhydrophobic surfaces (water contact angle  $\geq 150^\circ$ ) was then evaluated and 4 different types of nanostructures were found to be suitable – nanofin, nanopillar, ribbed nanograting and zig-zag rows of nanopillars. The water contact angles and relevant measurements are shown in Table I.

	Contact Angle	Cassie-Baxter Prediction	Roll-Off Angle	Contact Angle Hysteresis	Effect
Nanofins	153.3° ± 1.5°	150.2°	Parallel: 12.0° ± 1.4°	Parallel: 28.0° ± 4.2°	Rose Petal
			Perpendicular: 16.8° ± 1.1°	Perpendicular: 40.5° ± 3.5°	
Nanopillars	161.8° ± 1.8°	163.7°	3.3° ± 1.1°	3.5° ± 0.7°	Lotus Leaf

Ribbed Nanogratings	$154.3^\circ \pm 1.2^\circ$	$151.9^\circ$	-	Parallel: $43.0^\circ \pm 5.7^\circ$	Rose Petal
				Perpendicular: $70.8^\circ \pm 1.1^\circ$	
Zig-zag rows of nanopillars	$\approx 180^\circ$	$178.9^\circ$	$\approx 0^\circ$	$\approx 0^\circ$	Lotus Leaf

Table I: Measurements of superhydrophobicity exhibited by the various nanostructures. “Parallel” and “Perpendicular” refer to the water contact angles taken when the water droplet is spreading parallel and perpendicular to the long axis of the nanofins/ nanogratings respectively.

Of the 4 nanostructures, nanopillars and zig-zag rows of nanopillars mimic lotus leaf behavior (superhydrophobic with low roll-off angle)<sup>23</sup> whereas nanofins and ribbed nanogratings mimic rose petal behavior (superhydrophobic with high roll-off angle).<sup>24</sup> Note that 6  $\mu\text{l}$  water droplets do not roll off ribbed nanogratings even at  $90^\circ$ . The strong adhesion of droplets to ribbed nanogratings and nanofins is due to the relative abundance of nanostructure edges, which pin the triple phase contact line and cause the large contact angle hysteresis observed for these geometries<sup>25,26</sup> (Table I). In addition, both the nanofins and ribbed nanogratings exhibit axis-dependent wetting properties. The rise in contact angles from nanofins to ribbed nanogratings to nanopillars to zig-zag rows of nanopillars can be attributed to the increasing concentration of air spaces between the nanostructures as described by the Cassie-Baxter relation<sup>27</sup> (Table I).

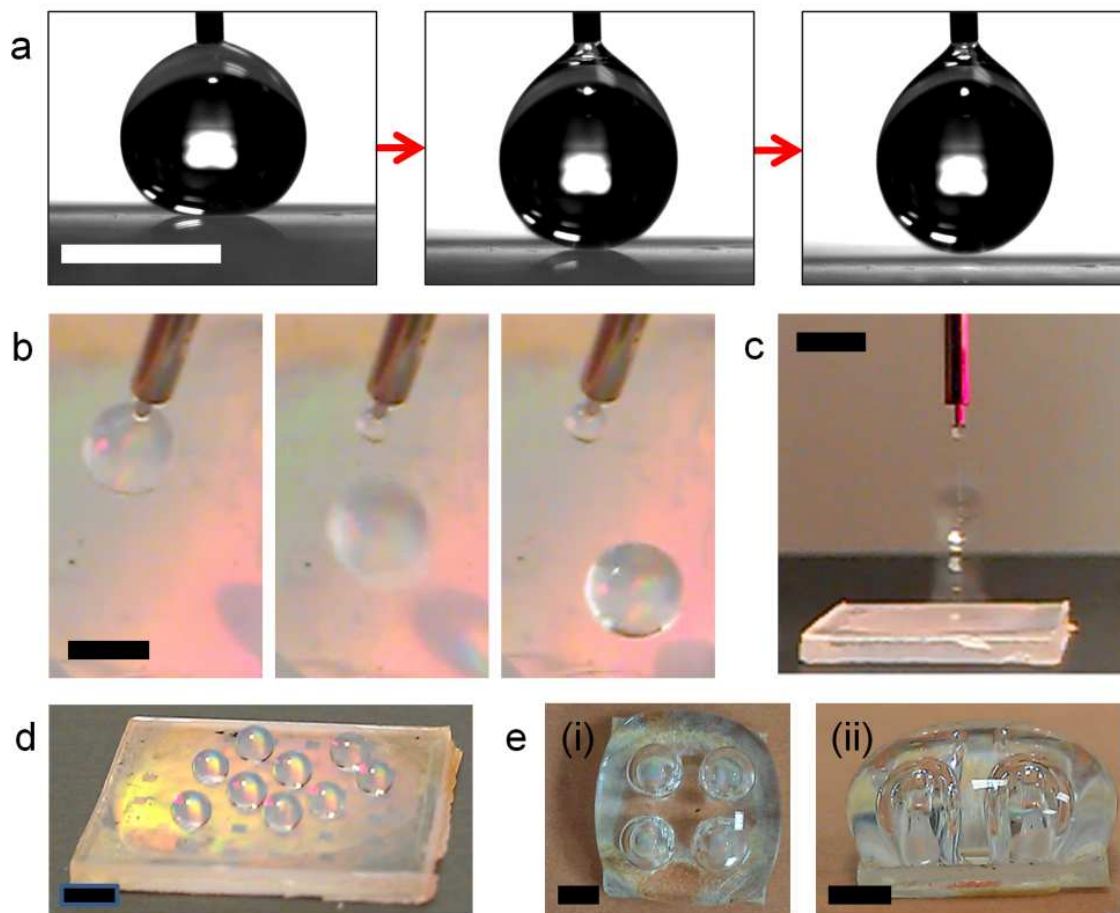


Figure 7: (a) Non-stick property of surface with zig-zag rows of nanopillars demonstrated with a 6  $\mu\text{l}$  water droplet. (b) Sliding of 6.4  $\mu\text{l}$  droplet over a distance of 3.5 mm on a level surface textured with zig-zag rows of nanopillars. (c) Bouncing 6.4  $\mu\text{l}$  droplet on zig-zag rows of nanopillars. (d) 1  $\mu\text{l}$  droplets trapped on 0.5 mm x 0.5 mm hydrophobic pads surrounded by superhydrophobic nanopillars. (e) (i) Top view and (ii) side view of 20  $\mu\text{l}$  of air bubbles trapped on 2 mm x 2 mm of superhydrophobic pads surrounded by hydrophilic untreated PS (water contact angle =  $83.5^\circ \pm 4.4^\circ$ ). Scale bars represent 2 mm.

It should be pointed out that the superhydrophobicity displayed by zig-zag rows of nanopillars is especially remarkable as droplets up to 6  $\mu\text{l}$  are not able to stick to the surface (see Figure 7a). When the volume of a freely suspended droplet reaches 6.4  $\mu\text{l}$ , its weight can

no longer be supported by the surface tension of the syringe tip and it falls. If this droplet is dropped onto a surface with zig-zag rows of nanopillars at a height of 2 mm (measured from bottom of suspended droplet to surface), it will have enough energy to travel several millimeters across the surface despite its weight (Figure 7b). When the height is raised to 7 mm, the droplet will acquire sufficient energy to bounce on the surface (Figure 7c). Based on these characteristics, it would appear that a surface modified with zig-zag rows of nanopillars obtained through low power plasma etching displays superhydrophobic properties on par with the very best reported in literature.<sup>28</sup>

A single substrate can be designed to have regions with superhydrophobic nanostructures and regions without nanostructures and are not superhydrophobic, so that the flow of water can be guided to specific positions. To demonstrate this, we created non-superhydrophobic PS pads surrounded by superhydrophobic PS nanopillars to trap water droplets (Figure 7d) and superhydrophobic PS pads (with nanostructures) surrounded by hydrophilic PS (without nanostructures) to trap air bubbles (Figures 7e and 7f). Note that all of these were integrated on a single substrate without requiring any surface coatings.

Given the extraordinary superhydrophobic properties exhibited by PS nanostructures fabricated through low power plasma etching and the ease with which these structures can be integrated into other designs, they will likely find extensive usage in applications such as self-cleaning surfaces and microfluidics. However, we have discovered decreasing hydrophobicity over time of our plasma treated PS, probably due to interaction with atmospheric oxygen<sup>29</sup> and/or moisture, so that continued study is required for improvement of the durability of the PS nanostructures for repeated usage.

### Nanoimprinting

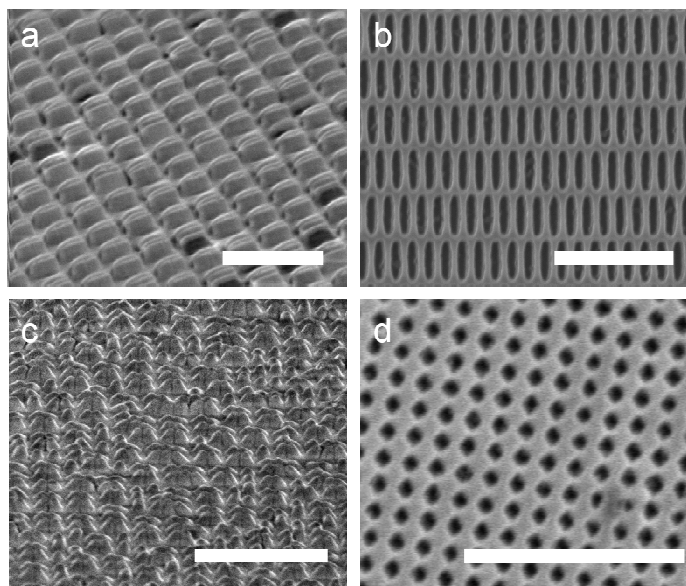


Figure 8: (a) PDMS nanofins fabricated from (b) PS mold of nanofin holes. (c) PDMS nanopillars fabricated from (d) PS mold of nanopillar holes. Scale bars represent 5 μm.

Another possible area of application would be the use of PS nanostructures as extremely cost-effective, non-brittle molds (as compared to silicon and quartz) for low temperature ( $\leq 90^{\circ}\text{C}$ ) nanoimprinting. By our estimates, silicon wafers are approximately 2000 times as expensive as PS wafers and this, therefore, provides a great impetus to drive down the cost of nanoimprinting by replacing mold material.

The feasibility of this idea is shown here using PDMS. As can be seen in Figure 8, the nanofins were faithfully reproduced according to the mold cavities. It is worth noting that pairing of PDMS nanofins and bunching of PDMS nanopillars have already occurred even though the aspect ratio of the nanostructures is only about 3, which is a direct result of the high array density.

### Biocompatibility and Neurite Guidance

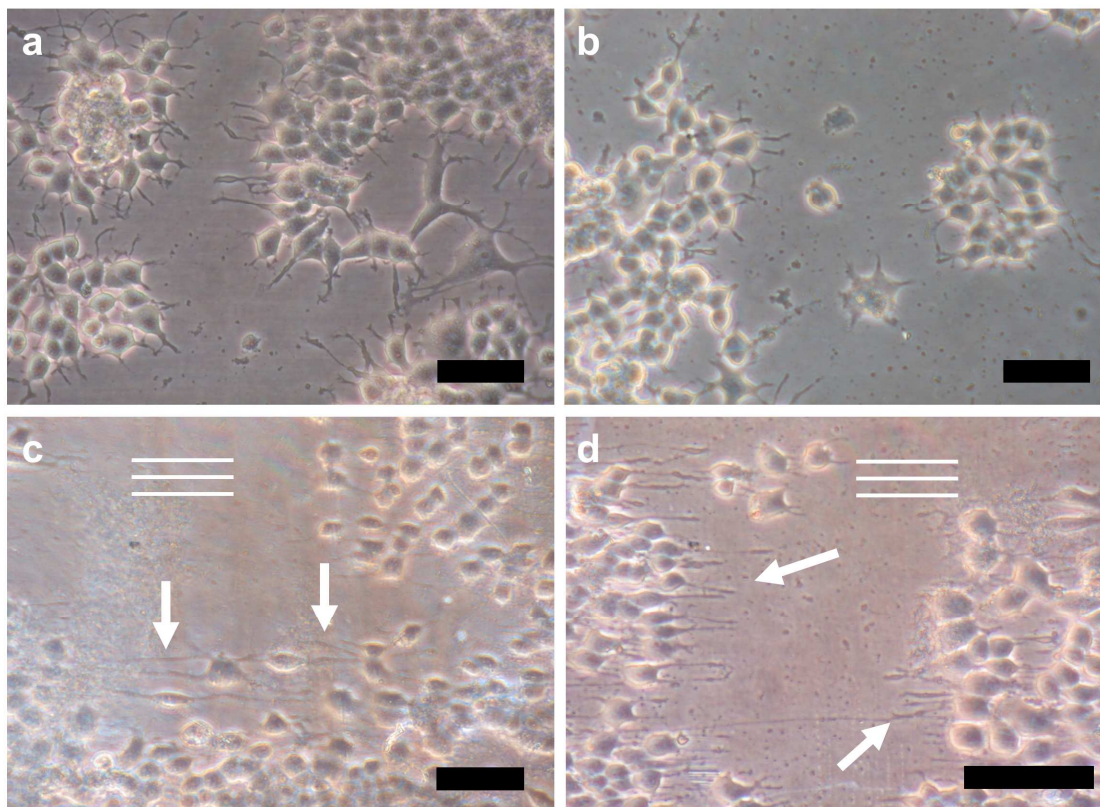


Figure 9. Representative photographs of neurite-directing with PS nanogratings. Cells on (a) culture well (b) unpatterned PS (c) nanogratings etched with pure oxygen plasma and (d) nanogratings etched with 50% O<sub>2</sub> plasma. The nanogratings are oriented horizontally in (c) and (d) as indicated by the white lines. White arrows point to the directed neurite growths. Scale bars represent 50 μm.

Exploiting the biocompatibility of PS, we also explored the possibility of plasma etched PS nanostructures in tissue engineering, specifically, in directing cell growth. PS nanogratings were fabricated with plasma compositions of 100% O<sub>2</sub> and 50% O<sub>2</sub> and

subjected to neurite directing experiments. Unpatterned PS from the compact disc cover and culture well served as experimental controls.

Although PC12 cells were able to proliferate and differentiate on both the culture well and unpatterned PS substrate, the neurites were not extended in any preferred direction (Figures 9a and 9b). In contrast, nerve cells on the patterned substrates in Figures 9c and 9d produced numerous parallel, elongated neurites as a result of the spatial anisotropy of nanogratings<sup>5</sup>, thus demonstrating the suitability of PS nanostructures in providing topographical cues to the cells to influence their growth behaviour. In addition, it was noted that PC12 cells on nanogratings etched with 50% O<sub>2</sub> plasma extended more developed neurites compared to those on nanogratings etched with pure O<sub>2</sub> plasma. This is likely a result of the different hydrophilicity of the plasma treated PS (See Supporting Information II) which is known to influence cell behaviour<sup>30,31</sup>. By controlling the surface chemistry through the plasma composition, therefore, the extent of cell proliferation can be manipulated as well.

## Conclusions

Low power CF<sub>4</sub>/O<sub>2</sub> plasma etching was investigated as an alternative method for nanostructuring polymer surfaces. The dependence of etch anisotropy on CF<sub>4</sub>/O<sub>2</sub> plasma gas composition was investigated and it was found that the gas composition influences the level of fluorination of the PS substrate and fluorocarbon deposition during plasma treatment, which in turn, affects the etch anisotropy and etch rate as fluorinated PS and the deposited fluorocarbon polymer are less susceptible to isotropic radical etching. We have shown that the CF<sub>4</sub>/O<sub>2</sub> plasma composition results in structures that can be divided into 4 distinct regimes, with each regime displaying a characteristic trend for etch anisotropy.

Stitch etching, a new concept that is based on “pre-patterning” and imperfect anisotropy in etching, was introduced to enhance the maximum height and therefore, surface

area of nanostructures. We showed that unusual nano-architectures such as ribbed nanogratings and zig-zag rows of nanopillars can be obtained using this technique.

We also demonstrated the versatility of our new fabrication technique in creating a wide range of patterns (nanopillar, nanofin and nanograting array) on different polymer substrates (Polystyrene, Polypropylene, Kapton® Polyimide, PET).

Lastly, the utility of our PS nanostructures was investigated and it was shown that PS nanostructures can be employed as cost-effective superhydrophobic surfaces, nanoimprinting molds and neurite directing substrates.

In conclusion, we find that low power plasma etching is a viable fabrication route for creating polymeric nanostructures with a wide range of useful engineering properties. It has the advantage of combining etching and surface functionalization in a single step and avoids issues related to molds, release coatings and high temperature processing, and is versatile enough to be applied to thermosetting polymers and uneven surfaces, both of which are incompatible with nanoimprinting. With these advantages, low power plasma etching should find extensive usage in nanotechnology research and manufacturing.

## **Acknowledgements**

We would like to thank Singapore-MIT Alliance for the financial support of this project, C.V. Thompson and W.K. Choi for their invaluable advice and guidance, Ze Liang Yuan for his assistance in XPS data acquisition and Walter Lim for providing his technical expertise in the use of various machines for this work.

## References

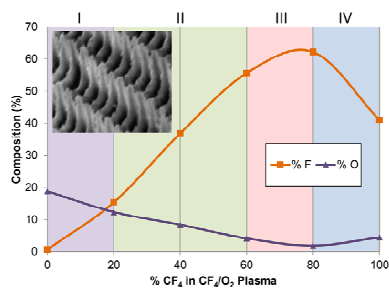
1. Shibata, S. Fabrication of high-resolution gratings for polymeric optical waveguide devices. in **5351**, 127–133 (SPIE, 2004).
2. Jeon, S. *et al.* Ultraviolet nanoimprinted polymer nanostructure for organic light emitting diode application. *Applied Physics Letters* **92**, 223307 (2008).
3. Guo, L. J., Cheng, X. & Chou, C.-F. Fabrication of Size-Controllable Nanofluidic Channels by Nanoimprinting and Its Application for DNA Stretching. *Nano Lett.* **4**, 69–73 (2003).
4. Hu, W., Yim, E. K. F., Reano, R. M., Leong, K. W. & Pang, S. W. Effects of nanoimprinted patterns in tissue-culture polystyrene on cell behavior. *J Vac Sci Technol A* **23**, 2984–2989 (2005).
5. Zhu, M. *et al.* Creation of nanostructures by interference lithography for modulation of cell behavior. *Nanoscale* **3**, 2723 – 2729 (2011).
6. Guo, L. J. Recent progress in nanoimprint technology and its applications. *Journal of Physics D: Applied Physics* **37**, R123–R141 (2004).
7. Geim, A. K. *et al.* Microfabricated adhesive mimicking gecko foot-hair. *Nat Mater* **2**, 461–463 (2003).
8. Chen, M.-H., Chuang, Y.-J. & Tseng, F.-G. Self-masked high-aspect-ratio polymer nanopillars. *Nanotechnology* **19**, 505301 (2008).
9. Korre, H., Fucetola, C. P., Johnson, J. A. & Berggren, K. K. Development of a simple, compact, low-cost interference lithography system. in **28**, C6Q20–C6Q24 (AVS, 2010).
10. Mogab, C. J., Adams, A. C. & Flamm, D. L. Plasma etching of Si and SiO<sub>2</sub>—The effect of oxygen additions to CF<sub>4</sub> plasmas. *Journal of Applied Physics* **49**, 3796 (1978).

11. Strobel, M., Corn, S., Lyons, C. S. & Korba, G. A. Surface modification of polypropylene with CF<sub>4</sub>, CF<sub>3</sub>H, CF<sub>3</sub>Cl, and CF<sub>3</sub>Br plasmas. *Journal of Polymer Science: Polymer Chemistry Edition* **23**, 1125–1135 (1985).
12. Occhiello, E., Morra, M., Gardassi, F. & Bargon, J. On the application of XPS, SSIMS and QCM to study the surface of a CF<sub>4</sub>/O<sub>2</sub> plasma treated polycarbonate. *Applied Surface Science* **36**, 285–295 (1989).
13. Egitto, F. D. Plasma etching and modification of organic polymers. *Pure and Applied Chemistry* **62**, 1699 – 1708 (1999).
14. Ahn, S. H. & Guo, L. J. High-Speed Roll-to-Roll Nanoimprint Lithography on Flexible Plastic Substrates. *Advanced Materials* **20**, 2044–2049 (2008).
15. Alvine, K. J. *et al.* Capillary instability in nanoimprinted polymer films. *Soft Matter* **5**, 2817–2972 (2009).
16. Hu, W., Crouch, A. S., Miller, D., Aryal, M. & Luebke, K. J. Inhibited cell spreading on polystyrene nanopillars fabricated by nanoimprinting and in situ elongation. *Nanotechnology* **21**, 385301 (2010).
17. Chang, S., Oh, J., Boles, S. T. & Thompson, C. V. Fabrication of silicon nanopillar-based nanocapacitor arrays. *Applied Physics Letters* **96**, 153108–153108–3 (2010).
18. Mai, T. T. *et al.* Dynamics of Wicking in Silicon Nanopillars Fabricated with Interference Lithography and Metal-Assisted Chemical Etching. *Langmuir* **28**, 11465–11471 (2012).
19. Lai, C. Q. *et al.* Influence of nanoscale geometry on the dynamics of wicking into a rough surface. *Applied Physics Letters* **102**, 053104–053104–4 (2013).
20. Bico, J., Tordeux, C. & Quéré, D. Rough wetting. *Europhysics Letters (EPL)* **55**, 214–220 (2001).

21. Lai, C. Q. *et al.* Droplet spreading on a two-dimensional wicking surface. *Phys. Rev. E* **88**, 062406 (2013).
22. Kogoma, M., Kasai, H., Takahashi, K., Moriwaki, T. & Okazaki, S. Wettability control of a plastic surface by CF<sub>4</sub>-O<sub>2</sub> plasma and its etching effect. *Journal of Physics D: Applied Physics* **20**, 147–149 (1987).
23. Neinhuis, C. & Barthlott, W. Characterization and Distribution of Water-repellent, Self-cleaning Plant Surfaces. *Ann Bot* **79**, 667–677 (1997).
24. Feng, L. *et al.* Petal Effect: A Superhydrophobic State with High Adhesive Force. *Langmuir* **24**, 4114–4119 (2008).
25. Lai, C. Q., Thompson, C. V. & Choi, W. K. Uni-, Bi-, and Tri-Directional Wetting Caused by Nanostructures with Anisotropic Surface Energies. *Langmuir* **28**, 11048–11055 (2012).
26. Paxson, A. T. & Varanasi, K. K. Self-similarity of contact line depinning from textured surfaces. *Nat Commun* **4**, 1492 (2013).
27. Cassie, A. B. D. & Baxter, S. Wettability of porous surfaces. *Transactions of the Faraday Society* **40**, 546 (1944).
28. Hsu, S.-H. & Sigmund, W. M. Artificial Hairy Surfaces with a Nearly Perfect Hydrophobic Response. *Langmuir* **26**, 1504–1506 (2010).
29. Petrat, F. M., Wolany, D., Schwede, B. C., Wiedmann, L. & Benninghoven, A. Comparative in situ ToF-SIMS/XPS study of polystyrene modified by argon, oxygen and nitrogen plasmas. *Surface and Interface Analysis* **21**, 402–406 (1994).
30. Pennisi, C. P., Zachar, V., Gurevich, L., Patriciu, A. & Struijk, J. J. The influence of surface properties of plasma-etched polydimethylsiloxane (PDMS) on cell growth and morphology. *Conf Proc IEEE Eng Med Biol Soc* **2010**, 3804–3807 (2010).

31. Valamehr, B. *et al.* Hydrophobic surfaces for enhanced differentiation of embryonic stem cell-derived embryoid bodies. *Proceedings of the National Academy of Sciences* **105**, 14459–14464 (2008).

## Table of Contents Graphic



Study of  $\text{CF}_4/\text{O}_2$  plasma chemistry's influence on polymeric nanostructure formation and application to superhydrophobic surfaces, nanoimprinting moulds and neuro-direct substrates.